

**Use Of Ionosonde Values Of The F2-Layer Maximum Electron Density (NmF2) To Study
Geophysical Equivalency Using Statistical Summaries**

Sapna Chouhan, Dr.Ram Mohan Singh Bhadoria

Research Scholar, Associate Professor

Department Of Physics

Sunrise Univerisity

Alwar

(Received:15June2020/Revised:10July2020/Accepted:22July2020/Published:28July2020)

Abstract

The most important pre-storm conditions for the mid-latitude ionosphere's response to geomagnetic storms are the season and the local time of the storm's commencement (SC). The combination of processes connected to solar production and magnetospheric input, respectively, is governed by the difference between a site's geomagnetic and geographic latitudes. Contextual analyses of explicit tempests utilizing ionospheric information from the two sides of the equator are innately overwhelmed via occasional impacts and the different nearby times versus longitude of the SCs. We define "geophysically-equivalent-sites" as locations in which the geographic and geomagnetic latitudes have the same relationship to one another in both hemispheres in order to investigate ionospheric consistency. Because the differences between geomagnetic and geographic latitudes are greatest at the longitudes of the dipole tilt, these are the best places to determine whether the hemispheres' preconditioning and/or storm-time input are the same or different. Using statistical summaries of 206 solar cycle #20 events, we use ionosonde values of the F2-layer maximum electron density (Nm F2) to investigate geophysical equivalency at Hobart (Tasmania) and Wallops Island (Virginia). Over seven-day storm periods, we construct average patterns of Nm F2 (percent) versus local time that better depict the average characteristics of ionospheric storms' positive and negative phases. Four local time characteristic patterns of storm-induced perturbations, as well as the average magnitudes and time scales of the processes that cause them in each hemisphere, are consistent with the findings.

Keywords: Ionosphere (turbulence in the ionosphere; Ionosphere at the mid-latitudes; General or random)

Introduction

The ionosphere of the Earth is disturbed by a variety of factors. During times of global geomagnetic storms, the effects are the most obvious and well-documented. Several types of F2-layer observations have been used to study the resulting "ionospheric storms": a) the maximum electron density measured

by an ionosonde (NmF2), b) the total electron content measured by a satellite radio beacon (TEC), c) the electron and ion densities, temperatures, and plasma dynamics measured by incoherent scatter radar (ISR), and d) satellite in situ measurements of ionosphere/thermosphere parameters along orbital tracks Prolss (1995) and Mendillo (2006) provided comprehensive summaries of storm effects in NmF2 and TEC, respectively, for ISR results by Buonsanto (1999) and satellite data by Prolss (1974). It has been possible to successfully model the fundamental morphologies and driving processes of ionospheric storms in various latitude zones. This brief summary almost always refers to the investigation of storm effects in the Northern Hemisphere. Ionospheric storm studies have been reintroduced as a major topic in aeronomy and solar-terrestrial physics in general thanks to the development of global positioning system (GPS) methods for observing TEC on a global scale. GPS methods have been most useful in the case-study approach to studying ionospheric storms (e.g., Foster and Rideout, 2005), providing a significantly improved capability for documenting perturbation patterns previously observed at only a few specific longitudes where ground-based station networks existed (e.g., Mendillo and Klobuchar, 1975, for 70 W). In addition, the sparse ionosonde network and absence of coherent scatter radars in the Southern Hemisphere have been significantly enhanced by the routine observation of the physical mechanisms that were previously thought to be agents during storms in both hemispheres.

Methodology

Utilizing 206 geomagnetic storms during solar cycle #20, our initial investigations of the concept of geophysically equivalent-sites—defined as locations in each hemisphere where geographic and geomagnetic latitudes are approximately equal or have the same difference—were carried out. At longitudes where the tilt of the geomagnetic axis maximizes the difference between geographic and geomagnetic latitudes, the ionosphere exhibits a consistent average response. An analysis that depicted perturbation effects as a function of hours following the start of the storm is used in this to demonstrate this. This allows the investigation to be extended to the depiction of diurnal effects, revealing consistency in the distinctive local time features that are associated with both the positive and negative phases. However, the positive phase is always slightly stronger at Wallops Island, whereas the negative phase is always deeper and lasts longer at Hobart, regardless of whether the patterns use all of the storms that are available or subsets by a specific category (such as the type of geomagnetic storm, the time of its sudden commencement, or the season). In contrast to straightforward seasonal differences between the hemispheres, we hypothesized that variations in storm input might be the cause of this. Could the electro-dynamical cycles that lead to the "nightfall impact" basically be more compelling in the Northern Side of the equator? Is the enhanced chemical loss of the negative phase attributed to the aurora heating effects being more pronounced in the Southern Hemisphere? When it comes to daytime

SC storms, why are the localized periods of enhanced depletions associated with trough motions more severe in the Northern Hemisphere than in the Southern Hemisphere? We considered the possibility that Wallops Island and Hobart are not precisely geophysically equivalent, but that Hobart experiences less production and more auroral heating due to its higher latitudes by 4–5 degrees. As outlined above for the asymmetry in the sea-sonal anomaly, we checked to see if this was the case by comparing summer and winter conditions at the two locations. This inferred that little geographic scope contrasts didn't contribute emphatically to the different pat-terns found. We looked at the pattern of ionospheric storm effects that occur during years of declining solar cycle conditions from the Christchurch, New Zealand, station (43.6°S, 172.8°E) to examine potential influences of geomagnetic latitude. As shown in Table 2, this location has a geomagnetic latitude of 50.3 degrees, which is nearly identical to that of Wallops Island in the north and is less than one degree from Hobart's. In this way the contrast between attractive geographic scopes is ~13°at Wallops, ~11°at Hobart, however just ~7°at Christchurch. The two Southern Hemisphere stations had very similar positive phases, both of which were smaller than at Wallops. As a result, the positive phase was not significantly affected by the differences in magnetic latitudes between our candidate geophysically equivalent sites—Wallops Island and Hobart. Hobart had deeper early storm depletions than Christchurch, as might be expected for a site at a higher geomagnetic latitude. The negative phases between Christchurch and Hobart were not the same. However, the phases of recovery were very similar. With local time results, we now address these issues. we choose the best (non-seasonal) conditions for ionospheric storm magnitudes: daytime SC events during years when the solar cycle is in its declining phase. There were 55 such occasions at Pummels Island and 39 at Hobart and 38 at Christchurch. However, due to subtle differences in latitude-dependent mechanisms, the three dusk effect patterns probably do show meaningful separations. The absence of a highly significant geomagnetic anomaly only in the Southern Hemisphere and the fact that the magnetic poles are not precisely aligned along a portion of the Earth's diameter are perhaps the most important of these. Last but not least, thermosphere winds and other non-electro dynamical mechanisms can be influenced by geomagnetic field geometry. The vertical component of enhanced winds, or pulse-like effects (Prolss, 1995), flowing from polar latitudes toward the equator has a control over magnetic field inclination (I) and declination (D). Table 1 shows that these parameters vary between the sites used, but their overall effect on vertical motions all show that horizontal winds have about a 30% vertical component. As a result, these parameters do not provide a discriminator that could suggest differences due to thermosphere dynamics. The geomagnetic field strength above Hobart and Wallops varies by 20 percent, which can have a significant impact on precipitation input and is independent of geometrical effects.

Positive Correlation Between Solar Wind Density and SME in the Saturation Regime: The Role of Density in Controlling Energy Transfer into the Ionosphere

It had been widely accepted for quite some time that the auroral electro jets were not controlled by sun-oriented breeze thickness [e.g., Murayama et al. 1980)]. The solar wind density was found to have a strong correlation with the AL and AU indices twice, as stated by Shue and Kamide (2001). On January 10, 1997, during the main phase of the geomagnetic storm during the southward IMF, the first period occurred (figure). On January 11, 1997, the second period included a 150 cm³-density, strongly northward IMF (figure). However, at the time, little was known about these relationships' physical origins. When the Mach number is low and the IMF is large-southward, saturation of the ionospheric potential occurs. This implies that the ionosphere's true capacity is generally delicate to changes in the IMF. Dayside merging will be accelerated by an increase in density because, under these conditions, the geoeffective length is inversely proportional to the density of the solar wind. As a result, there is a relationship between the solar wind density and the auroral intensity. Lopez and others (2004) use the LFM simulation to study the January 10 event (Shue & Kamide, 2001) and find the same behavior as shown in the figure. This work stands out because it was the first to show that MHD simulations could capture this effect.

In order to investigate the effect of solar wind density on the intensity of auroral electrojets in the saturation regime, we selected our storms for which the solar wind parameters were nearly constant during their main phase, with the exception of the density, which changed significantly. We present two tempest occasions, one with a low Mach number and the other with a customary Mach number, in the accompanying segments. The first storm occurred on June 1, 2013. The primary phase of this storm began at 1200 UTC and ended at 1900 UTC. In order to calculate the correlation between SME and solar wind density in this storm, we selected the time period between 0420-0700 UT, when the minimum of Dst is 152 nT. As can be seen in the figure, Bz remains roughly constant throughout this time period. Other parameters, such as density, of the solar wind remain essentially constant, and the Mach number is less than 4. When the lagtime between the solar wind data and the SME index is nine minutes, the figure's left panel at the top shows the highest correlation (0.71). The direct connection among SME and sun powered breeze thickness is portrayed in the figure's left board base.

Large-scale Magneto-Hydro-Dynamic (MHD) physics is the cause of this relationship between SME and solar wind density, so global MHD models should replicate data results. Consequently, to confirm this connection, we made use of the Space Weather Modeling Framework (SWMF) and the Community Coordinated Modeling Center (CCMC) storm event simulation. The SWMF simulation makes use of numerical models of the Inner Heliosphere, Solar Energetic Particles, Global Magnetosphere, Inner

Magnetosphere, Radiation Belt, Ionosphere, and Upper Atmosphere in a parallel, high-performance model (Gombosi et al., 2004). There are two versions of the SWMF model that are used on CCMC. v20180525 was the version that we used. SME-solar wind density is equivalent to the relationship between Joule heating and solar wind density because Joule heating is a scaled function of SME (see Chapter 3). Consequently, we established the connection between the solar wind density and the simulated joule heating of this event. As shown in figure 2-right board, we can see a comparative model from the SWMF multiplication; The joule heating power and the SW density have a high correlation of 0.67 when a five-minute lagtime is taken into account.

Left-Bottom Panel

The SME index in relation to solar wind density for the selected time period during the event on June 1, 2013. Top of right panel: The relationship coefficient between the sun based breeze thickness and the reproduced Joule warming control over the long haul.

Left-bottom panel: The simulated Joule heating in relation to the solar wind's density for a specific time frame during the event on June 1, 2013. On the other hand, the second storm with a regular Mach number occurred on December 20, 2015. We just think about the main segment of this twofold tempest. The fundamental stage of the first segment began at 0400 UT and ended at 1000 UT. Figure 3 shows that during this time, Bz has a large value and stays roughly the same, as do VBs and the total magnitude of B, but the Mach number has a median value of 6 and stays mostly the same. We chose the time period between 0610 and 0810 UT to calculate the correlation between SME and solar wind density. The minimum of Dst in the first part of this storm is 116 nT. This Mach number value therefore suggests that we are not within the saturation range. As shown in Figure 4, there is no relationship between the solar wind density and the SME index. Because the potential did not reach saturation, the merging interaction significantly regulates energy transfer into the ionosphere. The authors (Bruntz et al.), 2012), the viscous potential is approximately 78 kV on average and the reconnection potential is approximately 160 kV. There is some dependence on density (for a different reason than what was discussed with the force-balance model) because the viscous potential scales like n. Because the reconnection potential is higher than the viscous potential and is not saturated, there is no significant correlation between the density and SME.

Solar Wind And SM-Indices During The Event On 20 December 2015

We research 11 geomagnetic storms that are tantamount to the first depicted here. The IMF is large and moving south during these storms (table 1 summarizes).

Also, the Mach number is low. As a function of the average Mach number for each event over the specified time period, the correlation coefficient between the SME index and the solar wind density is

shown in Figure 5. As can be seen, as the Mach number decreases, the correlation coefficient becomes larger as the effect of density grows. This is because a lower Mach number leads to a more saturated ionospheric potential; Accordingly, the sun based breeze's different boundaries are less significant than the thickness of the sun oriented breeze in deciding the power of the auroral electrojet. Consequently, there is a stronger correlation between the SME index and changes in the solar wind density. We can reason that the sun based breeze thickness is a significant control factor for how much energy that enters the ionosphere during storms with low Mach numbers.

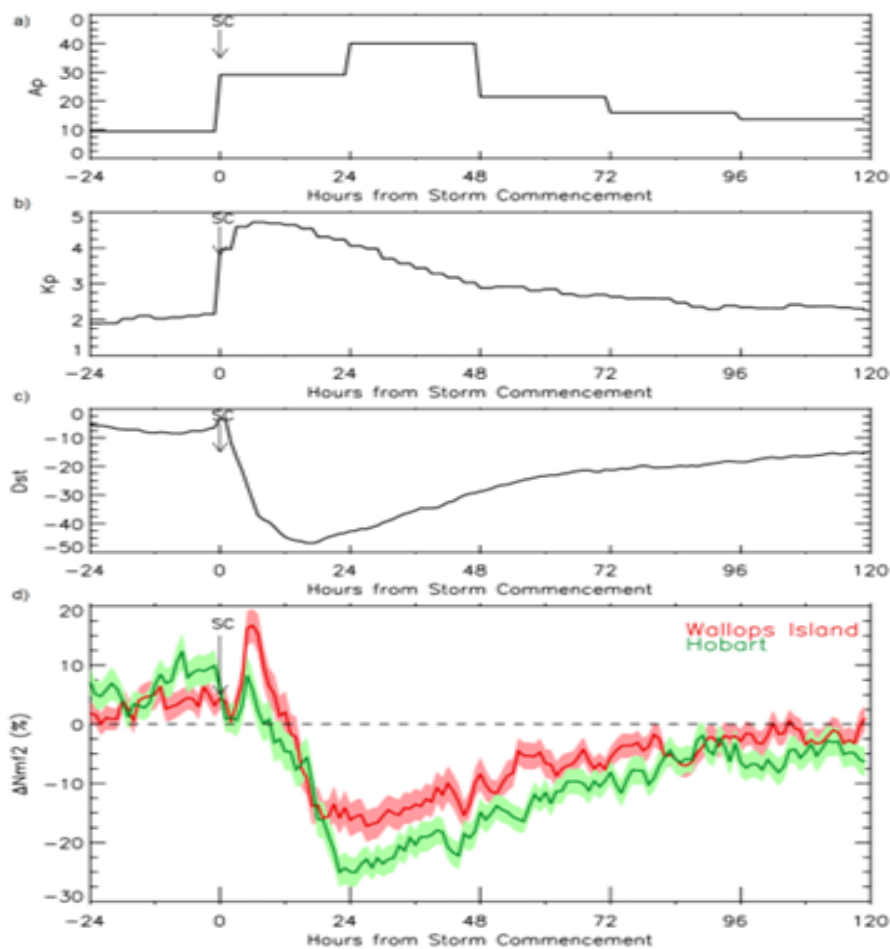


Fig. 1. Average patterns obtained from 206 geomagnetic storms during solar cycle #20 (October 1964–June 1976) for geomagnetic indices and ionospheric behavior versus hours following a storm commencement (SC). In panel (a) the daily index A_p is shown, in (b) the 3-h index K_p , and in (c) the hourly index Dst . Collectively they portray the classic behavior of a large-scale geomagnetic storm. In panel (d), the ionospheric response as obtained using hourly ionosonde values of maximum electron density ($NmF2$) in percentage change from the monthly mean are shown for the geophysically-equivalent-sites of Wallops Island (VA) and Hobart (Tasmania). The shadings give the uncertainties of

the means for the computed patterns, defined as the standard deviation of the mean divided by the square root of the sample size.

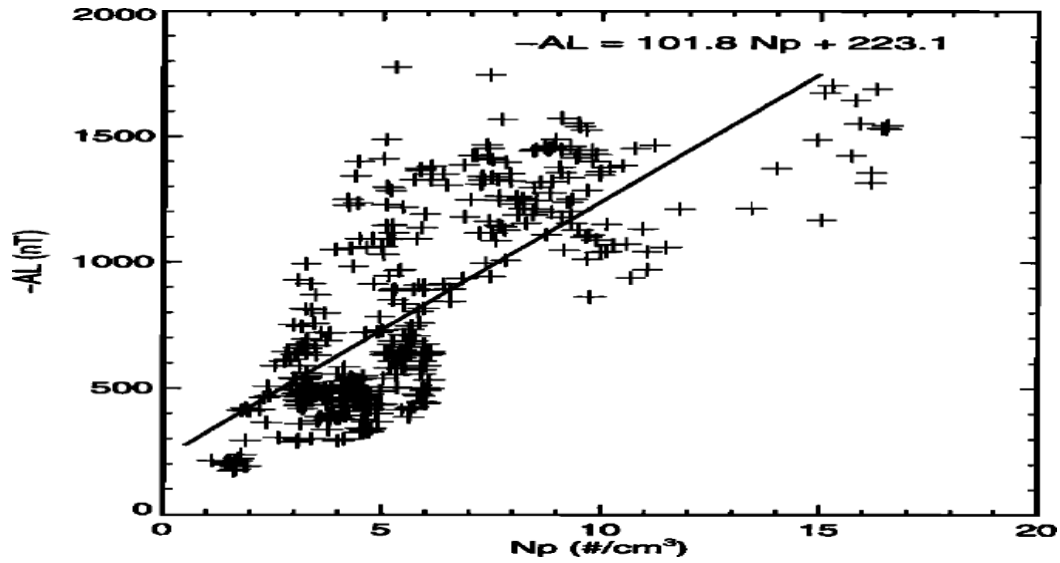


Figure 2: Shue and Kamide's correlation coefficient between the January 10, 1997, AL index and solar wind density.

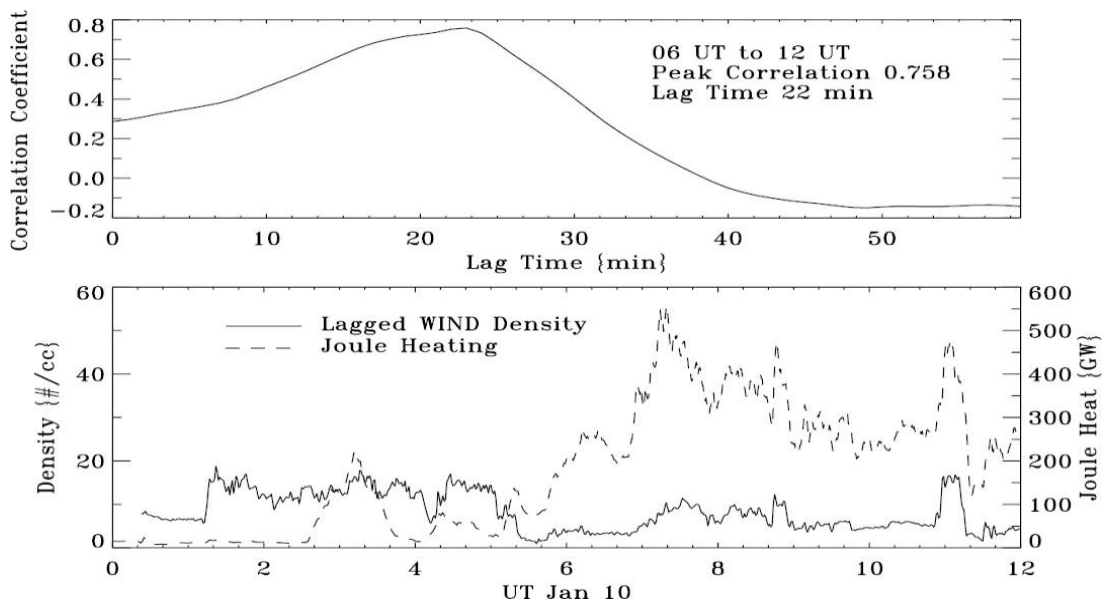


Figure 3: Lopez and others 2004) investigate the January 10 event using the LFM simulation: The simulation's integrated Joule heating in the northern ionosphere and the solar wind density are depicted in the bottom panel. The correlation between solar wind density and Joule heating as a function of lag time is depicted in the top panel for the time period from 0600 UT to 1200 UT. Zero lag is the time when solar wind entered the grid upstream of the bow shock.

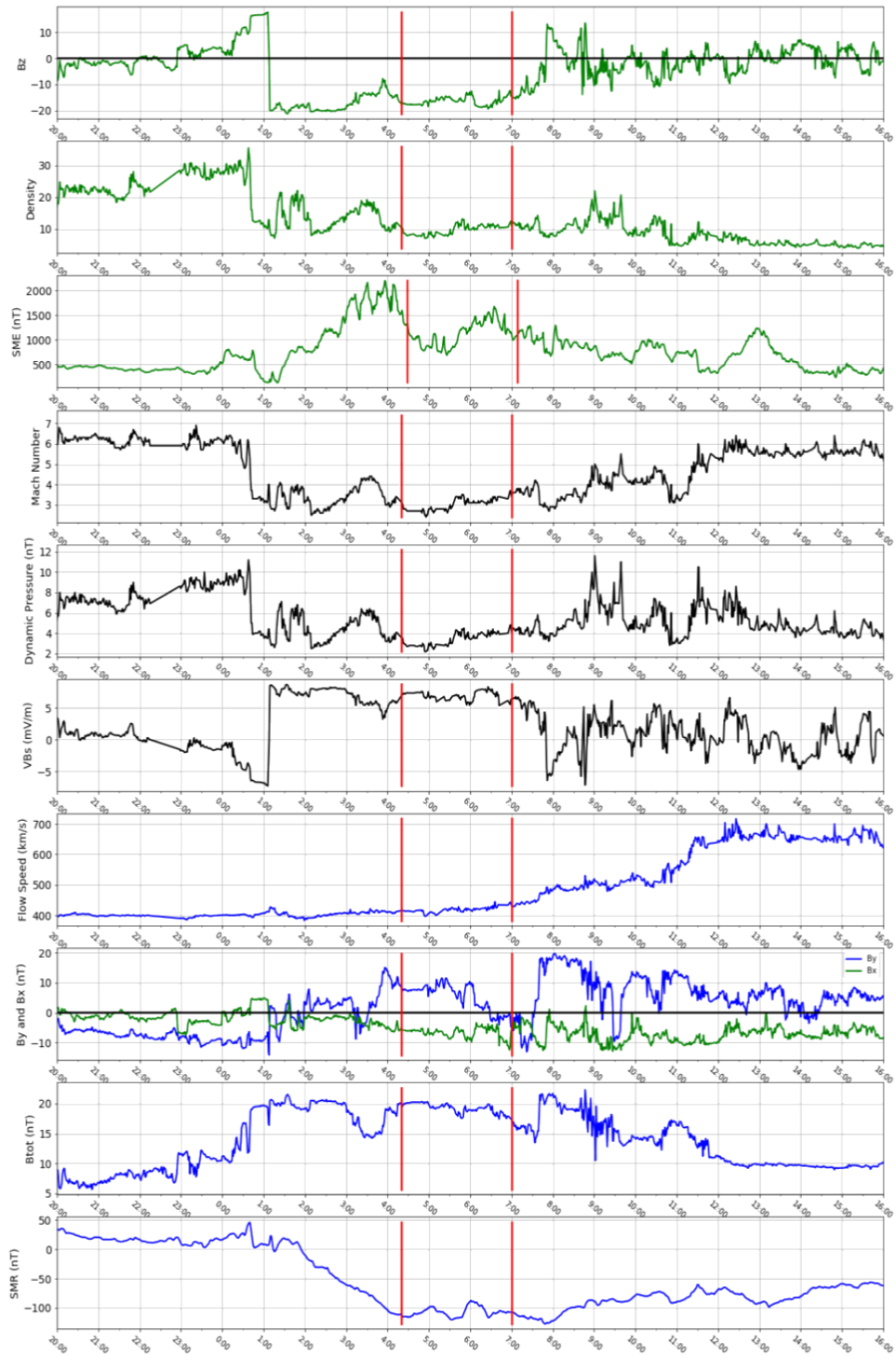


Figure 4: OMNI and SuperMAG data for the event 1 Jun 2013. The period between red lines is the selected period for this event.

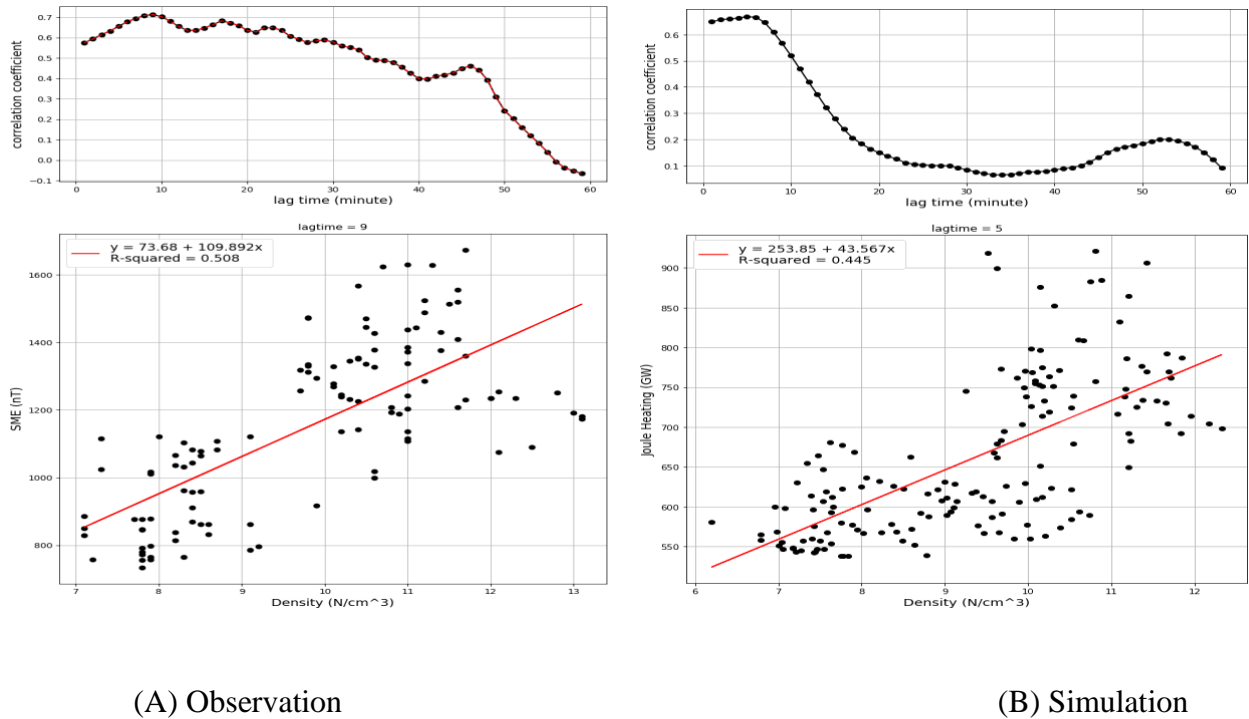


Figure 5: Top of left panel: The lagtime-dependent correlation coefficient between the SME index and the solar wind density.

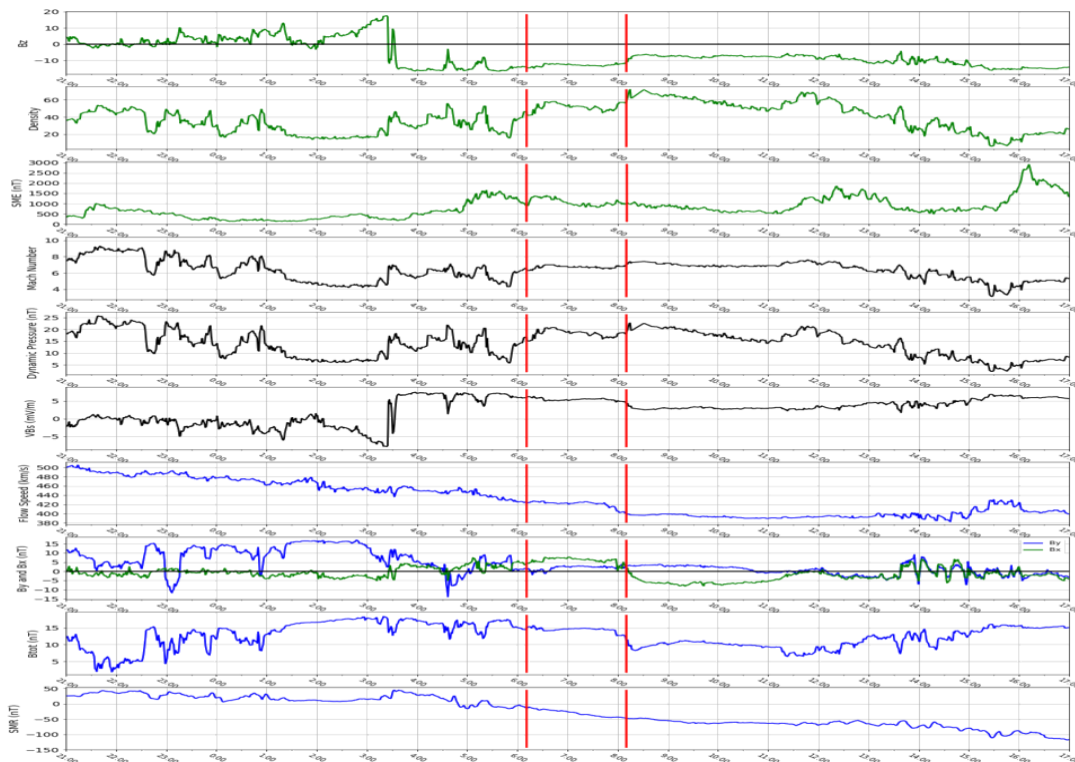


Figure 6: Omni And Supermag Data For The Event 20 December 2015. The Period Between Red Lines Is The Selected Period For This Event.

Date	Time of Main Phase	min <i>Dst</i> *	Selected Period
10 January 1997	06-12 UT	-87 nT	0600-1200 UT
20 August 1998	07-20 UT	-84 nT	1000-1400 UT
13 November 1998	05-22 UT	-150 nT	0700-0930 UT
28 Feb.-1 March 1999	17-01 UT	-122 nT	1800-2030 UT
13 November 1999	12-23 UT	-122 nT	1800-2100 UT
14 October 2000	02-15 UT	-127 nT	1100-1420 UT
3 October 2001	06-15 UT	-187 nT	0915-1115 UT
26-27 June 2004	22-03 UT	-142 nT	0900-1250 UT
30 May 2005	06-14 UT	-138 nT	0715-1015 UT
1 June 2013	01-09 UT	-152 nT	0420-0700 UT
27 August 2014	03-19 UT	-103 nT	0930-1330 UT

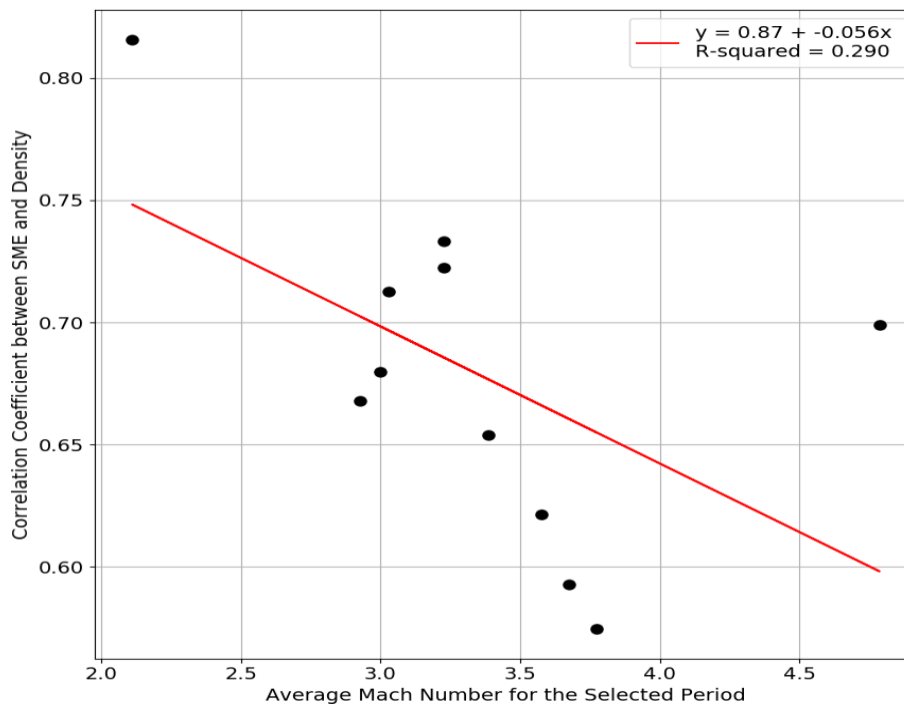


Figure 8: The ratio of the Sme Index to the average Mach number for the selected time period of each event to the solar wind density. The data's linear fit to the red line indicates that a lower Mach number is associated with a stronger correlation.

Conclusion

Using geophysically nearly identical stations, we investigated in depth the local time effects of ionospheric storm perturbations. Similar storm patterns emerge when a wide range of initial conditions are considered. This loans backing to the idea of geophysically-comparable locales in the two sides of the equator. However, there are a few instances of minor but persistent variations that point to possible hemispheric asymmetries in the processing of storm-time energy input within this context of consistency. Based on the findings presented here, it appears that the local time disturbance patterns produced by the analysis techniques developed here are the most appropriate for such discussions. Local time-dependent mechanisms for the positive phase (winds, electric fields, and precipitation) and the negative phase (daytime O/N2 changes, nighttime trough motions) may then be more directly related to the characteristic disturbance patterns that were found. Our tracking down that generally little errors in accurate geophysically-comparable conduct happened during sun based cycle #20 should be sought after utilizing different blends of same-half of the globe and double side of the equator station matches during something very similar and other sun oriented cycles.

References

- [1].Berényi, K.A., Kis, Á., Heilig, B., Urbář, J. and Barta, V., 2022, May. Comprehensive analysis of the response of the ionospheric F2-layer to the largest geomagnetic storms from solar cycle# 24 over Europe. In EGU General Assembly Conference Abstracts (pp. EGU22-2309).
- [2].Mendillo, M., Narvaez, C. and Marusiak, A.G., 2013. Are ionospheric storms the same during different solar cycles?. *Journal of Geophysical Research: Space Physics*, 118(10), pp.6795-6805.
- [3].Vijaya Lekshmi, D., Balan, N., Tulasi Ram, S. and Liu, J.Y., 2011. Statistics of geomagnetic storms and ionospheric storms at low and mid latitudes in two solar cycles. *Journal of Geophysical Research: Space Physics*, 116(A11).
- [4].Liu, W., Xu, L., Xiong, C. and Xu, J., 2017. The ionospheric storms in the American sector and their longitudinal dependence at the northern middle latitudes. *Advances in Space Research*, 59(2), pp.603-613.
- [5].Balan, N., Yamamoto, M., Liu, J.Y., Otsuka, Y., Liu, H. and Lühr, H., 2011. New aspects of thermospheric and ionospheric storms revealed by CHAMP. *Journal of Geophysical Research: Space Physics*, 116(A7).

- [6].Berényi, K.A., Barta, V. and Kis, Á., 2018. Midlatitude ionospheric F2-layer response to eruptive solar events-caused geomagnetic disturbances over Hungary during the maximum of the solar cycle 24: A case study. *Advances in Space Research*, 61(5), pp.1230-1243.
- [7].Mansilla, G.A. and Zossi, M.M., 2016. Some ionospheric storm effects at an Antarctic station. *Advances in Space Research*, 57(6), pp.1319-1327.
- [8].Danilov, A.D., 2013. Ionospheric F-region response to geomagnetic disturbances. *Advances in Space Research*, 52(3), pp.343-366.
- [9].Uryadov, V.P., Vybornov, F.I., Kolchev, A.A., Vertogradov, G.G., Sklyarevsky, M.S., Egoshin, I.A., Shumaev, V.V. and Chernov, A.G., 2018. Impact of heliogeophysical disturbances on ionospheric HF channels. *Advances in Space Research*, 61(7), pp.1837-1849.
- [10]. De Abreu, A.J., Martin, I.M., Fagundes, P.R., Venkatesh, K., Batista, I.S., de Jesus, R., Rockenback, M., Coster, A., Gende, M., Alves, M.A. and Wild, M., 2017. Ionospheric F-region observations over American sector during an intense space weather event using multi-instruments. *Journal of Atmospheric and Solar-Terrestrial Physics*, 156, pp.1-14.
- [11]. Liu, J., Liu, L., Zhao, B. and Wan, W., 2012. Influence of interplanetary solar wind sector polarity on the ionosphere. *Journal of Geophysical Research: Space Physics*, 117(A8).
- [12]. Ippolito, A., Perrone, L., Plainaki, C. and Cesaroni, C., 2020. Investigating the foF2 variations at the Ionospheric Observatory of Rome during different solar cycles minimums and levels of geomagnetic activity. *Journal of Space Weather and Space Climate*, 10, p.52.
- [13]. WU, J.S. and XU, L., 2015. Statistical study of the ionospheric storms over 5 latitude zones in the European sector. *Chinese Journal of Geophysics*, 58(2), pp.349-361.
- [14]. Kakoti, G., Bhuyan, P.K., Kalita, B.R. and Baruah, A.A., Climatology of Conjugate Hemisphere Ionospheric Response to Geomagnetic Storms along 95 E during Solar Cycle 24.
- [15]. Devi, M., Patgiri, S., Barbara, A.K., Gordiyenko, G., Depueva, A., Depuev, V. and Ruzhin, Y.Y., 2018. Storm time ionospheric-tropospheric dynamics: A study through ionospheric and lower atmospheric variability features of high/mid and low latitudes. *Geomagnetism and Aeronomy*, 58, pp.857-870.